

# 1st Adiabatic Invariants and Phase Space Densities for the Jovian Electron and Proton Radiation Belts-Galileo and GIRE3 Estimates

Henry Berry Garrett<sup>1</sup> and Insoo Jun<sup>2</sup>

<sup>1</sup>California Institute of Technology

<sup>2</sup>Jet Propulsion Lab (NASA)

November 26, 2022

## Abstract

The fluxes and phase space densities for a fixed 1<sup>st</sup> adiabatic invariant for high energy electrons and protons provide important inputs for various scientific studies for determining the physics of particle diffusion and energization. This study provides estimates of the 1<sup>st</sup> adiabatic invariant and phase space density based on the complete and large data base available from the Energetic Particle Detector (EPD) on Galileo for the jovian environment. To be specific, 10 minute averages of the high energy electron and proton data are used to compute differential flux spectra versus energy for  $L \sim 8 - 25$  over the Galileo mission. These spectra provide estimates of the differential fluxes and phase space density for constant 1<sup>st</sup> adiabatic invariants between  $10^2$  to  $10^5$  MeV/G. As would be expected, the electron and proton fluxes and phase space densities generally trend lower as the planet is approached. The results indicate that, whereas the overall trends for each orbit are consistent, detailed orbit to orbit variations can be observed. Galileo orbit C22 is presented as a specific example of deviations from the mean downward trend. To validate the Galileo results and extend the findings into  $L=3$ , the GIRE3 model was also used to compute the fluxes and phase space densities for constant 1<sup>st</sup> adiabatic invariant versus L-shell. Comparison between GIRE3 and EPD demonstrates that the model adequately reproduces the EPD data trends and they consistently show additional variations near Io. This provides proof that the GIRE3 is a useful starting point for diffusion analyses and similar studies.

1 **1<sup>st</sup> Adiabatic Invariants and Phase Space Densities for the Jovian**  
2 **Electron and Proton Radiation Belts—Galileo and GIRE3 Estimates**

3  
4 **H. B. Garrett<sup>1</sup> and I. Jun<sup>1</sup>**

5 <sup>1</sup>The Jet Propulsion Laboratory, California Institute of Technology

6  
7 Corresponding author: Insoo Jun (Insoo.Jun@jpl.nasa.gov)

8  
9 **Key Points:**

- 10 • The long-term dynamics of particle trapping in the Jovian magnetosphere is investigated  
11 using high energy electron and proton data.
- 12 • 1<sup>st</sup> adiabatic invariant and phase space densities are computed using the EPD data as well  
13 as using the GIRE3 model.
- 14 • Both electrons and protons show a clear downward trend in flux and PSD at constant 1st  
15 adiabatic invariant as the planet is approached.
- 16  
17

## 18 **Abstract**

19

20 The fluxes and phase space densities for a fixed 1<sup>st</sup> adiabatic invariant for high energy  
21 electrons and protons provide important inputs for various scientific studies for determining the  
22 physics of particle diffusion and energization. This study provides estimates of the 1<sup>st</sup> adiabatic  
23 invariant and phase space density based on the complete and large data base available from the  
24 Energetic Particle Detector (EPD) on Galileo for the jovian environment. To be specific, 10  
25 minute averages of the high energy electron and proton data are used to compute differential flux  
26 spectra versus energy for  $L \sim 8 - 25$  over the Galileo mission. These spectra provide estimates of  
27 the differential fluxes and phase space density for constant 1<sup>st</sup> adiabatic invariants between  $10^2$  to  
28  $10^5$  MeV/G. As would be expected, the electron and proton fluxes and phase space densities  
29 generally trend lower as the planet is approached. The results indicate that, whereas the overall  
30 trends for each orbit are consistent, detailed orbit to orbit variations can be observed. Galileo  
31 orbit C22 is presented as a specific example of deviations from the mean downward trend. To  
32 validate the Galileo results and extend the findings into  $L=3$ , the GIRE3 model was also used to  
33 compute the fluxes and phase space densities for constant 1<sup>st</sup> adiabatic invariant versus L-shell.  
34 Comparison between GIRE3 and EPD demonstrates that the model adequately reproduces the  
35 EPD data trends and they consistently show additional variations near Io. This provides proof  
36 that the GIRE3 is a useful starting point for diffusion analyses and similar studies.

37

## 38 **Plain Language Summary**

39 Long term high-energy radiation environment at Jupiter is studied in this paper by using  
40 an extensive data set collected by the Galileo Energetic Particle Detector (EPD). This is the first  
41 time that the EPD high energy data are used in its entirety for this purpose. The results from the  
42 long-term ( $\sim 7$  years) observation confirm that trapped protons and electrons are indeed diffusing  
43 inward to the planet although there are some short-term orbit-to-orbit variations. This finding is  
44 shown to be consistent with the GIRE3 model output which has been and is being used for  
45 various Jovian mission designs (e.g., Juno, Europa Clipper, Europa Lander Concept Study)

46

47

## 48 **1 Introduction**

49

50 The last four decades have seen a significant increase in in-situ data on the jovian  
51 radiation belts. Following the Pioneer and Voyager flybys, Galileo observed the belts from 1995  
52 through 2005 with 34 complete orbits. Recently, the Juno spacecraft has begun another long  
53 term mission to this kind of planets. Unique to the various jovian missions, however, Galileo  
54 primarily orbited near Jupiter's equatorial plane with the bulk of its measurements at distances  
55 greater than  $\sim 8$  R<sub>J</sub>. Juno in contrast is primarily in a high inclination orbit with very low perijove  
56 flybys over the jovian poles—it will largely miss the radiation belts until late in its mission.  
57 Thus the Galileo data are of real value in mapping the equatorial radiation belts between 8 to 25  
58 R<sub>J</sub>—the region of particular interest to this study. To date, the Galileo data form an important  
59 data base for determining the physics of particle diffusion and energization in Jupiter's intense  
60 radiation belts (e.g., Nenon et al., 2018). Such studies are very dependent on the detailed  
61 variations of the fluxes and the phase space densities (PSD) at a constant 1<sup>st</sup> adiabatic invariant  
62 for high energy electrons and protons. To meet this need, the objective of this study is to provide  
63 estimates of the 1<sup>st</sup> adiabatic invariant fluxes and phase space densities based on the John

64 Hopkins Applied Physics Laboratory’s (JHU/APL) Energetic Particle Detector (EPD)  
65 experiment (see Williams et al., 1992) on Galileo for high energy electrons in the range 0.1  
66 MeV—100 MeV and protons between 0.6 MeV—100 MeV. (Note: The EPD data used here are  
67 from the “real time” collection mode and do include “record mode” collection mode data taken  
68 near the moons.)  
69

70 To be specific, 10-minute averages of the EPD electron data channels are averaged to  
71 provide omni-directional differential fluxes at 0.238, 0.416, 0.706, 1.5, 2.0, 11.0, and 31 MeV  
72 (the latter energy based on Pioneer 10 and 11 measurements) and between 3.2-10.1 MeV for  
73 protons between  $L \sim 8$  and  $L=25$  for the 34 Galileo orbits. These allow determination of spectra  
74 which provide estimates for the differential fluxes and for the PSD for constant 1<sup>st</sup> adiabatic  
75 invariants between  $10^2$  MeV/G to  $10^5$  MeV/G along Jupiter’s magnetic equator. The results  
76 permit studies of long term overall trends and orbit to orbit variations of these parameters. To  
77 illustrate the latter, the Galileo orbit C22 event is studied and provides valuable information on  
78 short period time variability.  
79

80 An important additional tool in the analysis of the radiation environment at Jupiter is the  
81 GIRE family of plasma and high energy particle models (e.g., Divine and Garrett, 1983; Garrett  
82 et al. 2003, 2005, 2012, 2015, 2016; de Soria-Santacruz et al., 2016, 2017; Jun et al., 2019). The  
83 latest version of the GIRE3 model (Garrett et al., 2017; Jun et al., 2019) is an amalgam of  
84 synchrotron measurements and Pioneer, Voyager, and Galileo in-situ data. GIRE3 provides a  
85 definition of the electrons, protons, and various heavy ions between  $\sim 2 R_J$  and  $50 R_J$  and for  
86 energies of a few eV to several 100 MeV/nucleon. Here GIRE3 will be used to compute the 1<sup>st</sup>  
87 adiabatic invariant and PSD versus  $L$  over the same range as the EPD data. GIRE3 also permits  
88 estimates of these key parameters into  $3 R_J$  and of their variations near Io. Though the  
89 agreement between the EPD data and model is not unexpected as GIRE3 is based in part on the  
90 EPD data, it provides further proof that GIRE3 is a useful tool for diffusion analyses and similar  
91 studies and for evaluating the latest models of losses and sources in the critical inner radiation  
92 belts (see for example Woodfield et al., 2014).  
93

94 This study is divided into two parts. First will be the computation of the 10 minute  
95 electron and proton fluxes and the PSD for fixed values of the 1<sup>st</sup> adiabatic invariant between  $\sim 8$   
96 and  $25 L$  for the Galileo data. These were broken out by orbit to study temporal variations—an  
97 example of which, orbit C22, will be presented. In the second part we will carry out a similar  
98 analysis using the GIRE3 model between  $L \sim 3$  and  $L=25$ . The electron and proton flux and  
99 phase space density contours versus energy are also computed to identify the applicable range of  
100 the analysis (i.e., between  $\sim 100$  keV to 100 MeV for the electrons and  $\sim 600$  keV to 100 MeV for  
101 the protons). Finally, the GIRE3 model and EPD variations with  $L$  will be compared and the  
102 results summarized.  
103

## 104 **2 Galileo Energetic Particle Detector (EPD)** 105

106 The primary data source for this analysis is the Galileo APL/JHU EPD Low-Energy  
107 Magnetospheric Measurement System (LEMMS) which measures the high energy electrons and  
108 protons from Jupiter orbit insertion (JOI) in 1995 to the end of the mission in 2005 (Williams et  
109 al., 1992). Specifically, the steps undertaken to analyze Jupiter’s trapped radiation in the jovian

110 magnetic equatorial plane in the range ~8 to ~25 Jupiter radii (1 jovian radius = 71,400 km)  
 111 using the Galileo EPD data are described in this section. First, the 10-minute averages of the  
 112 high-energy particle count rate data were combined with data on the location and magnetic field  
 113 at the spacecraft—specifically, the position of the Galileo spacecraft and the magnetic field  
 114 vector as modeled by the VIP4 magnetic field model (Connerney et al., 1998) from 8 to 25 L (L-  
 115 shell, rather than  $R_J$ , was used in this study as the data are better ordered in terms of the magnetic  
 116 field). Of the 32 LEMMS channels, the most important ones for radiation modeling are the  
 117 electron channels B1 (1.5-10.5 MeV), DC2 ( $\geq 2$  MeV, and DC3 ( $\geq 11$  MeV) and the proton  
 118 channel B0 (3.2-10.1 MeV). In addition, the F1 (174-304 keV), F2 (304-527 keV), and F3 (527-  
 119 884 keV) channels were included for lower energy electrons. To provide an upper bound on the  
 120 spectra at the highest energies, Pioneer 10 and 11 31 MeV measurements were added. Figure 1  
 121 is a plot of all the “raw” Planetary Data System (PDS) DC3 counts per second and the B0  
 122 differential fluxes to illustrate the variations of the EPD data with L-shell—over-plotted are the  
 123 variations for Galileo orbit C22.

124

125 Consider first the electrons. The 7 EPD and 1 P10/11 electron channel count rates were  
 126 converted to differential fluxes and fit with a spectrum of the form (Garrett et al., 2012):

127

$$128 \quad J(E) = J_0 E^{-A} \left(1 + E/E_0\right)^{-B} \quad (1)$$

129 where:

130  $J$  = Isotropic differential electron flux as a function of  $E$ ; ( $\text{cm}^2\text{-s-sr-MeV}$ )<sup>-1</sup>

131  $E$  = Electron energy; MeV

132  $J_0$  = Constant; ( $\text{cm}^2\text{-s-sr-MeV}$ )<sup>-1</sup>

133  $A$  = Constant (approximately the power law index for the low-energy component)

134  $B$  = Constant ( $A+B$  is approximately the power law index for the high-energy  
 135 component)

136  $E_0$  = Constant (approximately the breakpoint energy between low- and high-energy  
 137 spectra); MeV

138

139 The constants  $J_0$ ,  $A$ ,  $B$ , and  $E_0$  were computed for each 10 minute interval using EPD and  
 140 Pioneer data from the PDS. As will be discussed below, the Eq. 1 constants then define a flux  
 141 spectrum at each position that yields the electron 1<sup>st</sup> adiabatic invariant fluxes and the PSD  
 142 functions.

143

144 Whereas computing the high energy electron flux spectra for the EPD data as just  
 145 described was straightforward, computing the proton flux spectra was more involved. The  
 146 primary reason is that the high energy electrons inwards of 25 R<sub>J</sub> were found to contaminate the  
 147 high energy EPD proton channels except for the B0 3.2-10.1 MeV channel (Jun et al, 2002). A  
 148 proton flux spectrum in energy between 600 keV to 100 MeV is required to compute the fluxes  
 149 and power spectral density for a specified 1<sup>st</sup> adiabatic invariant at a given point. Our method to  
 150 do this assumes an appropriate proton spectrum scaled by the measured B0 flux at the point to  
 151 the energy desired. Fortunately, APL has provided reference proton and heavy ion differential  
 152 intensity spectra [Mauk et al., 2004] at 13 locations along the Galileo trajectory. These  
 153 differential spectra, interpolated in L, are assumed to represent the shape of the proton flux  
 154 distribution along the magnetic equator (Garrett et al., 2015). All the EPD ion data channels

155 between ~50 keV to ~50 MeV were simultaneously fit by APL to differential intensity spectra of  
 156 the form given in Eq. (2) (Mauk et al., 2004):

$$157$$

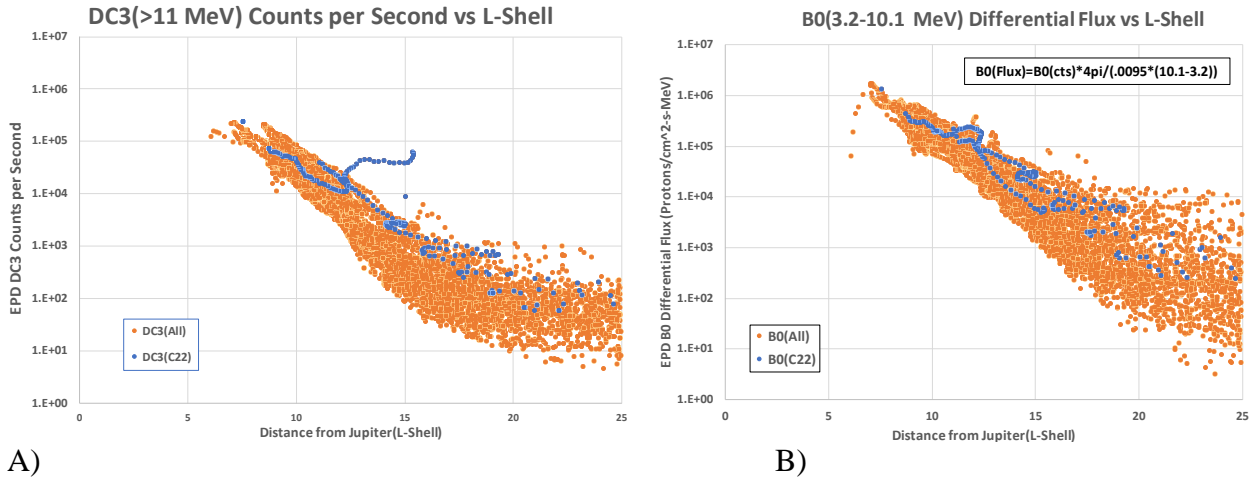
$$158 \quad J(E)_{APL} = C \frac{E[E_1 + kT(1 + \gamma_1)]^{-1 - \gamma_1}}{1 + (E_1/et)^{\gamma_2}} \quad (2)$$

159 where:

161  $C, et, kT, \gamma_1, \gamma_2$  = Parameters for the APL spectral fits to the EPD data at 13 locations  
 162 (Mauk et al., 2004; Eq. (1))

163  $E_1$  = Energy in reference frame of moving plasma (assumed =  $E$  in this study)

164



165 A)  
 166 B)  
 167 Fig. 1. 10 minute averages of EPD observations for A) the DC3 electron channel counts and B) the B0 proton  
 168 differential flux channel versus L-shell distance from Jupiter for all 34 orbits in orange. Also shown is orbit C22  
 169 (blue).

170  
 171 As described in Garrett et al. (2015), the selected APL proton spectra were interpolated in  
 172 L between ~8—25 L. The resulting spectra were then scaled by the observed B0 flux at the  
 173 desired point as derived from the PDS data. The estimated B0 fluxes (i.e.,  $J(B0)_{PDS}$ ) are plotted  
 174 in Figure 1 and were computed as follows:

$$175$$

$$176 \quad J(B0)_{PDS} = \frac{B0(cts) \cdot 4\pi}{GF \cdot (10.1 \text{ MeV} - 3.2 \text{ MeV})} \quad (3)$$

177 where:

179  $J(B0)_{PDS}$  = B0 channel isotropic differential proton flux based on observed  
 180 count rates;  $(\text{cm}^2\text{-s-MeV})^{-1}$

181  $B0(cts)$  = 10-minute averages of the B0 channel available from the PDS;  
 182 (counts per second)

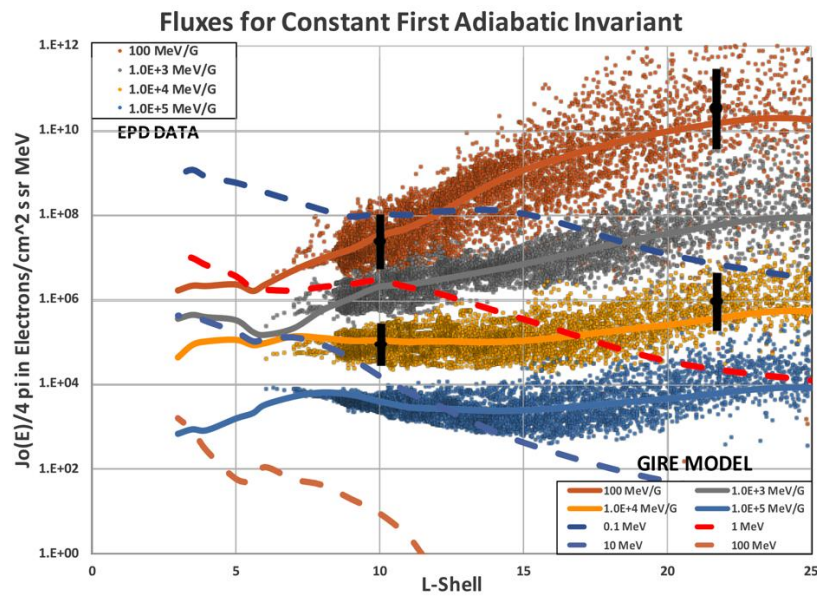
183  $GF$  = Average Geometric Factor for B0 Channel; ~0.0094  $\text{cm}^2\text{-sr}$  between  
 184 3.2–10.1 MeV (Jun et al., 2002)

185

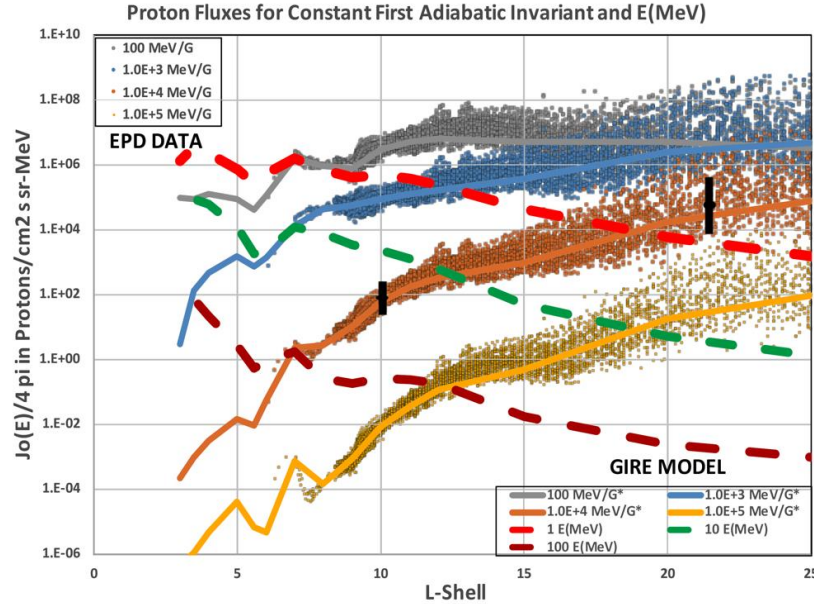
186 To scale the proton distribution at an arbitrary energy at a given B0 data location, the  
 187 GIRE3 model was exploited. As the GIRE3 proton model is based on the APL spectra (Garrett  
 188 et al., 2015), the spectra given by Eq. (2) as interpolated in L are readily recovered at a given



233 The procedure is to first define a value for  $I$  (e.g.,  $10^2$  MeV/G,... $10^5$  MeV/G) for the  
 234 electrons or protons. Eq. 7 then gives  $E$  for  $I$  and  $B_{eq}$  where  $B_{eq}$  is a function of L-shell and is  
 235 given for each EPD data point. The differential flux for the electrons or protons at  $L$  is next  
 236 computed for the value of  $E$  for the corresponding  $I$  and  $B_{eq}$ . L-shell and  $B_{eq}$  are computed using  
 237 the VIP4 magnetic field model (Connerney et al., 1998). Results are plotted in Figures 2 and 3  
 238 for electrons and protons respectively for all Galileo orbits (note: the EPD data are plotted as  
 239 dots, the solid and dashed lines are for the GIRE3 model and will be discussed in the next  
 240 section). For reference, vertical black lines at  $L=10$  and  $22$  in Figures 2 and 3 indicate the  
 241 uncertainty (assumed to be +/- one standard deviation of the mean of the log of the fluxes in a 2  
 242 L bin interval) in the first adiabatic invariant (see also Jun et al. (2005) for a statistical error  
 243 analysis of the EPD high energy electron data). This uncertainty varies from a factor of x2 inside  
 244 12 L to a factor of x6 to x10 at 24 L.  
 245  
 246



247  
 248  
 249 Fig. 2. Plot of 10 minute EPD electron fluxes for constant 1<sup>st</sup> adiabatic invariant  $I$  between  $10^2$  MeV/G to  $10^5$   
 250 MeV/G. Fluxes at constant  $I$  at similar values as determined by the GIRE3 model (solid lines) are also plotted. For  
 251 reference, GIRE3 flux contours for constant energies between 0.1 MeV and 100 MeV, the assumed range of validity  
 252 of the electron EPD data, are also shown as dashed lines.  
 253



254  
 255 Fig. 3. Plot of 10 minute EPD proton fluxes for constant values of the 1<sup>st</sup> adiabatic invariant  $I$  between  $10^2$  MeV/G  
 256 to  $10^5$  MeV/G. Also plotted are contours of constant  $I$  at similar values as determined by the GIRE3 model (solid  
 257 lines). For reference, GIRE3 flux contours for constant energies between 1 MeV and 100 MeV are also shown as  
 258 dashed lines (the EPD proton data are assumed to be valid between  $\sim 0.6$  MeV and  $\sim 100$  MeV).  
 259

260 The Galileo results are plotted for L values between L-shells of 8-25. The 25 L limit is  
 261 imposed as a result of how the jovian plasma disc is modeled. While it is straightforward to  
 262 compute values beyond  $\sim 25$  L, the  $B_{eq}$  values in particular are very dependent on the magnetic  
 263 field model assumed and L loses its relevance. Here the VIP4 model (Connerney et al., 1998) is  
 264 assumed as opposed to the plasma sheet models of Khurana et al. (2005) which are used in the  
 265 outer magnetosphere. The magnetic field models agree well inside 20 L but deviate significantly  
 266 beyond  $\sim 25$  L because of the complexities brought about by the jovian plasma disk.  
 267

268 The EPD data energy range of validity is also bounded as the flux contours for constant  $I$   
 269 indicate. That is, the EPD electron detectors are most reliable from  $\sim 170$  keV (the EPD F1  
 270 channel lower energy) to  $\sim 30$  MeV (the Pioneer 10 and 11). Even though the proton spectra  
 271 provided by Mauk et al. (2004) were fit between  $\sim 50$  keV to  $\sim 50$  MeV, the validity of EPD low  
 272 energy proton limit is estimated to be  $\sim 0.6$  MeV (Garrett et al., 2015). At the high energy end,  
 273 we have extrapolated both ranges up to 100 MeV, however, to allow for comparisons with the  
 274 GIRE3 model inside L=10.  
 275

276 While the general trend of both the electrons and proton fluxes for the EPD constant 1<sup>st</sup>  
 277 adiabatic invariants is towards lower values as the planet is approached, the electrons decrease  
 278 by only 1 order of magnitude or less between 25 L and 8 L for  $10^4$  MeV/G to  $10^5$  MeV/G while  
 279 the protons decrease by 2 orders of magnitude. Indeed, the EPD  $10^4$  MeV/G and  $10^5$  MeV/G  
 280 electron 1<sup>st</sup> adiabatic constant fluxes are almost flat over this region and even rise slightly inside  
 281 10 L.  
 282

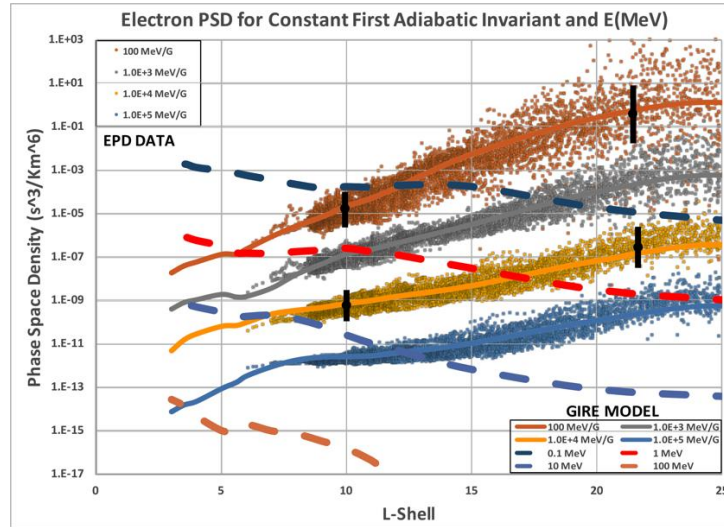
283 The second parameter of interest is the PSD. The PSD for relativistic particles is given  
 284 explicitly (for constant 1<sup>st</sup> adiabatic constant  $I$ ) by (e.g., Roederer, 1970; McIlwain and Fillius,  
 285 1975):

286  
 287  
 288  
 289  
 290  
 291  
 292  
 293  
 294  
 295

$$F(I) = J'(I)/P'(I)^2 \tag{8}$$

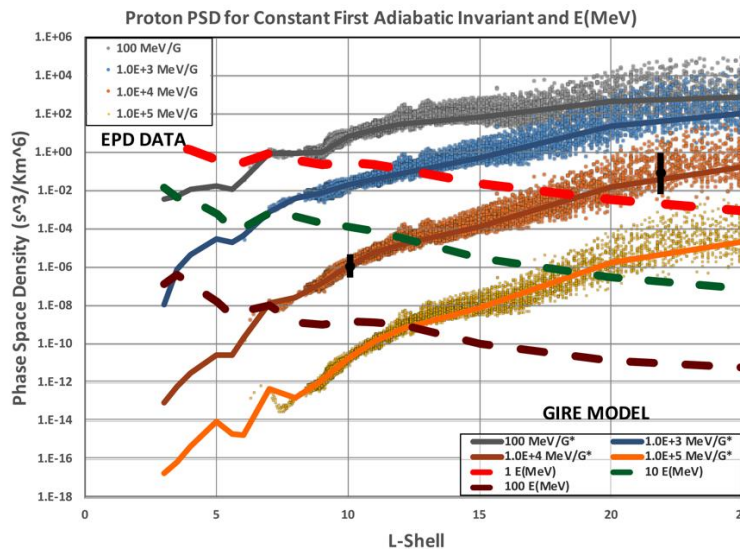
where:

- $F$  = PSD as a function of constant  $I$  for either electrons or protons;  
 Note:  $F'$  is plotted in Figs. 4 and 5 where  $F' = F \text{ m}^3$  assuming that units of  $F'$  are  $\text{s}^3/\text{km}^6$
- $J'$  = Isotropic differential flux as a function of  $E$ ;  $[\text{cm}^2\text{-s-sr-MeV}]^{-1}$
- $P'$  = Relativistic momentum, assumed to be  $P_{\perp}^2$  here;  $P_{\perp}$  is in units of  $\text{MeV}/c$



296  
 297  
 298  
 299  
 300  
 301

Fig. 4. Plot of 10 minute individual Galileo EPD electron PSDs for constant values of the 1<sup>st</sup> adiabatic invariant  $I$  between  $10^2$  MeV/G to  $10^5$  MeV/G. Additionally plotted are contours of constant PSD at similar values as determined by the GIRE3 model (solid lines). GIRE3 PSD contours for constant energies between 0.1 MeV and 100 MeV are also shown as dashed lines (see Fig. 2).



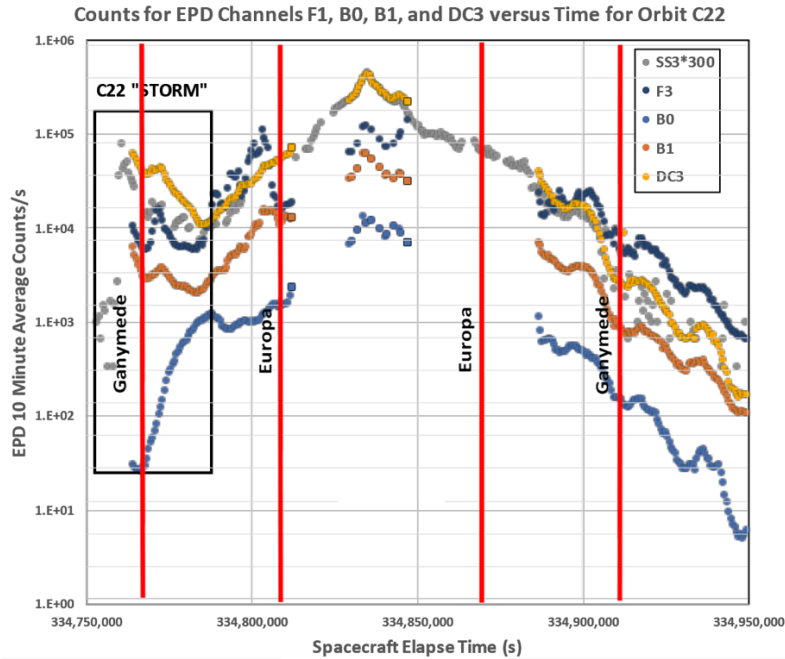
302  
 303  
 304  
 305  
 306

Fig. 5. Plot of 10 minute individual Galileo EPD proton PSDs for constant values of the 1<sup>st</sup> adiabatic invariant  $I$  between  $10^2$  MeV/G to  $10^5$  MeV/G. Additionally plotted are contours of constant PSD at similar values as determined by the GIRE3 model (solid lines). For reference, GIRE3 PSD contours for constant energies between 1 MeV and 100 MeV are also shown as dashed lines (see Fig. 3).

307  
308 The PSD is very important for determining the sources and losses in the diffusion  
309 equation (Woodfield et al., 2014). For Jupiter, it is assumed that the main source of the trapped  
310 high energy particles is the inward diffusion and energization of lower energy particles (assumed  
311 to be the high energy tail of the plasma particles streaming outward in the equatorial plane) from  
312 outside  $\sim 25 R_J$ . The evidence for this inward diffusion in Figures 4 and 5 is the steady decrease  
313 of the PSD as one approaches the planet for both the electrons and protons. This has been  
314 reported by many authors for Jupiter such as McIlwain and Fillius (1975), Baker and Goertz  
315 (1976), Mogro-Campero and Fillius (1976), Thomsen et al. (1977), Cheng et al. (1983, 1985),  
316 and Woodfield et al. (2014). While the electron PSD falls off smoothly with L-shell, a slight  
317 flattening of the fall-off in the proton curves is visible where the PSD data have a small  
318 inflection between  $\sim 12 L$  and  $\sim 17 L$  (particularly in the  $10^5$  MeV/G contour). This is possibly  
319 associated with Ganymede near  $15 L$  and, if the particles are infusing inward, may indicate it is a  
320 possible source of particles. There also appears to be a more rapid drop off at  $\sim 9 L$  that may  
321 represent absorption of inwardly diffusing particles by Europa. As for Figures 2 and 3, vertical  
322 black lines at  $L=10$  and  $22$  in Figures 4 and 5 indicate the uncertainty (assumed to be  $\pm$  one  
323 standard deviation of the mean of the log of the fluxes in a  $2 L$  bin interval) in the first adiabatic  
324 invariant. This uncertainty varies from a factor of  $\times 2$  inside  $12 L$  to a factor of  $\times 6$  to  $\times 10$  at  $24 L$ .

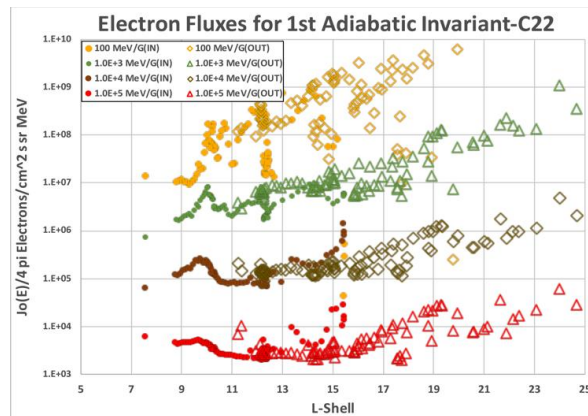
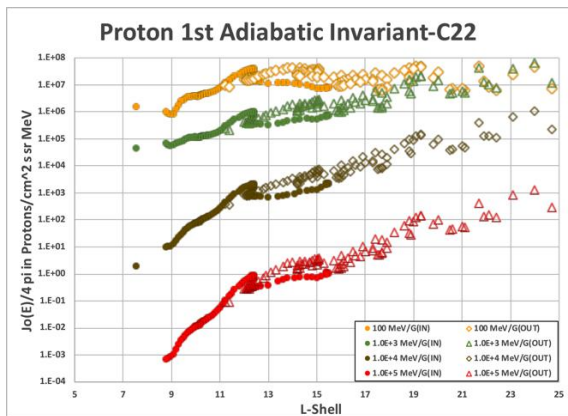
325  
326 The Galileo data can also be analyzed orbit by orbit. Although each of the orbits studied  
327 exhibit unique variations, orbit C22 (the 22<sup>nd</sup> orbit targeted for Callisto) is the most unusual as a  
328 major intensification of the high energy electrons was observed on Day 223 of 1999 as Galileo  
329 approached Jupiter. To illustrate the time evolution of the C22 observations, several of the EPD  
330 raw channels used in this study are plotted in Figure 6. The approximate duration of the C22  
331 event is marked. Unfortunately, the EPD was not turned on sufficiently in advance to determine  
332 when the event actually started and it may have been in progress well before the data collection  
333 began. Also shown in Figure 6 are data from the Galileo Star Scanner which fill in the gaps in  
334 the EPD data (note: the Star Scanner also apparently did not record the beginning of the event).  
335 When available, the Star Scanner data typically parallel the DC3 count rates as it is apparently  
336 sensitive to high energy electrons (Fieseler et al., 2002). The Star Scanner data in Figure 6 imply  
337 that there were no other “unusual” impulses following the initial one. Finally, the periodic  
338 oscillations in the count rates are the results of the oscillations of the jovian magnetic field—  
339 plotting the data in terms of L-shell largely removes these variations.

340



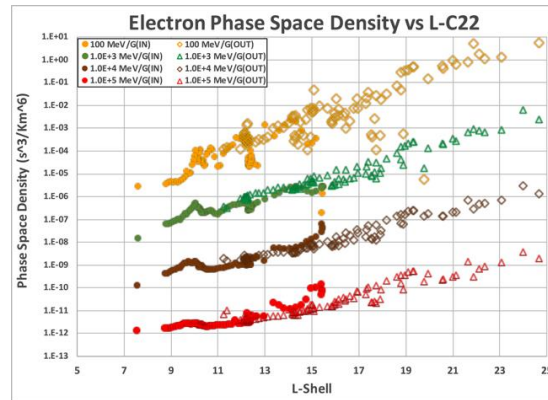
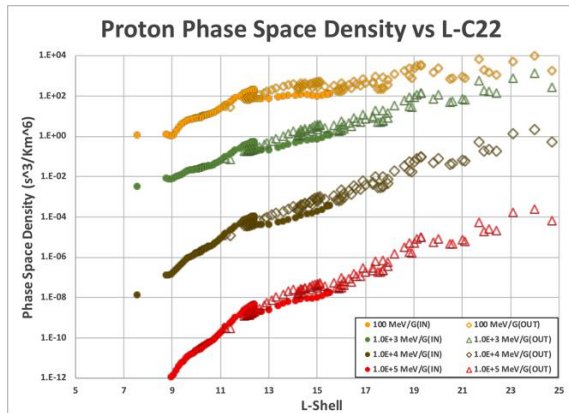
341  
 342 Fig. 6. Plot of 10 minute EPD counts per second for electron channels F3 (527-884 KeV), B1 (1.5-10.5 MeV), and  
 343 DC3 ( $E \geq 11$  MeV) and for proton channel B0 (3.2-10.1 MeV) for Galileo orbit C22. Also shown are the count rates  
 344 for the Galileo Star Scanner (SS3) for the same time period scaled by x300. Time is shown as spacecraft elapsed  
 345 time in seconds. The C22 “storm” interval is indicated by a box on the left. The times at which Galileo passed  
 346 through the orbits of Europa and Ganymede are indicated but do not necessarily mean it flew by them.  
 347

348 Figure 7 plots the proton and electron fluxes and PSDs as functions of L-shell. The data  
 349 are also divided into inward and outward portions of the C22 orbit (closed markers for inward  
 350 and open markers for outward). While the protons show a bump at around 12 L, they basically  
 351 follow the same trends in L as Figures 3 and 5. The electrons, however, show enhancements  
 352 between 9-10 L near Europa and near L=15 (corresponding to the initial C22 impulse  
 353 observation) for both the fluxes and PSDs (though 9-10 L impulse is much lower for the PSDs).  
 354 These features are unique to the C22 orbit electrons. The enhancement between 9-10 L might  
 355 indicate a source at Europa’s orbit or perhaps an outwardly propagating enhancement near Io that  
 356 is being shadowed by Europa—there is insufficient data inside 9 L to decide.  
 357



358  
 359 A.

B.



C.

D.

Fig. 7. Plots of the 10 minute averages of the particle fluxes and PSD versus L-shell for the Galileo C22 orbit corresponding to Fig. 6. A) is a plot of the proton fluxes for constant 1<sup>st</sup> adiabatic invariants; B) is a plot of the electron fluxes for constant 1<sup>st</sup> adiabatic invariants; C) is a plot of the proton PSD for constant values of 1<sup>st</sup> adiabatic invariant; D) is a plot of the electron PSD for constant 1<sup>st</sup> adiabatic invariant.

### 3 GIRE3 Model Results

In this section, the GIRE3 model will be exploited to evaluate the electron and proton fluxes and phase space densities for constant 1<sup>st</sup> adiabatic invariant with the intent of comparing the model and EPD results. The GIRE family of jovian models has been used for some time (Divine and Garrett, 1983; Garrett et al. 2003, 2005, 2012, 2015, 2016; de Soria-Santacruz et al., 2016, 2017; Jun et al., 2019) to evaluate the radiation environment at Jupiter. As mentioned, the GIRE3 model is an amalgam of synchrotron measurements and Pioneer, Voyager, and Galileo in-situ data. The full model provides a definition of the electrons, protons, and various heavy ions between  $\sim 2 R_J$  and  $50 R_J$  and for energies from a few eV to several 100 MeV/nucleon. Here the model is used to compute differential fluxes between 0.1 MeV and 100 MeV for the electrons and 0.6 MeV and 100 MeV for protons at selected energies versus L. The results in terms of constant 1<sup>st</sup> adiabatic invariant are converted to fluxes and PSDs for comparison with the EPD results. These are plotted as overlays in Figures 2, 3, 4, and 5 as solid lines. As would be anticipated since the GIRE3 model is based in part on the EPD data, there is agreement between 8 L and 25 L—the model appears to trace the mean of the EPD 10 minute electron and proton constant 1<sup>st</sup> adiabatic invariants. The comparisons provide proof that GIRE3 is a useful reference for diffusion analyses and for evaluating the latest models of losses and sources in the critical inner radiation belts.

To investigate the role of the jovian moons Io and Europa on the 1<sup>st</sup> adiabatic invariant flux and the PSD as modeled by GIRE3, the GIRE3 model was run into 3 L. The results are shown as overlays in Figs. 2, 3, 4, and 5 as solid lines. While for electrons the  $10^2$ ,  $10^3$ , and  $10^4$  MeV/G 1<sup>st</sup> adiabatic invariant fluxes appear to show structure near L-shells associated with Io (5-6 L) in Figure 2, there is minimal evidence for it in the  $10^5$  MeV/G (Figure 2) and the PSD plots (Figure 4). Indeed the GIRE3 contour plots imply that the PSDs drop off fairly smoothly inside the orbit of Europa into L=3. In contrast the protons show definite structure inside L=8. Both in Figures 3 and 5, there appears to be an initial increase around 7 L followed by a drop into 5-6 L followed by another increase and then a fall off inside Io's orbit. Io may be acting as a block for the inward diffusing protons. These latter variations may be suspect for portions of the  $10^4$  and

397  $10^5$  MeV/G  $1^{\text{st}}$  adiabatic invariant proton contours, however, as the GIRE3 predictions occur at  
398 energies above the 100 MeV proton energy contour (i.e., the dark red/purple dashed line which  
399 indicates the approximate upper energy bound of 100 MeV of the GIRE3 model).

400

#### 401 **4 Summary and Conclusion**

402

403 The objective of this paper was to investigate the variations in the flux and PSD at  
404 constant  $1^{\text{st}}$  adiabatic invariant between  $L \sim 8$  and  $L=25$  in the jovian equatorial plane for the  
405 high energy electrons and ions over the Galileo mission using the JHU/APL EPD data. Thus, the  
406 results reported in this paper represents a general long-term trend of particle trapping in the  
407 jovian radiation belts. In addition, the results were compared with the GIRE3 jovian particle  
408 model. The latter allowed the analysis to be extended into  $L \sim 3$ . As illustrated in Figures 2, 3, 4,  
409 and 5, the general trend of the electron and proton fluxes and PSDs for a given  $1^{\text{st}}$  adiabatic  
410 invariant was to decrease from  $L=25$  to  $L=3$ . This is generally assumed to indicate the inward  
411 diffusion and energization of the electrons and protons and is consistent with current  
412 observations and understanding of the sources of the jovian radiation belts. A new finding in this  
413 study is the more rapid fall off (factor of 100) in the fluxes or the PSDs of the protons with  $L$  as  
414 compared to the electrons. While the electrons and protons show gradual changes in slope  
415 between Ganymede and Europa, the protons show much higher order variations between 10  $L$   
416 and 3  $L$  (i.e., near the locations of Europa and Io).

417

418 The Galileo data set also allows the study of individual orbits. One example, the iconic  
419 C22 orbit presented here, shows detail in the  $1^{\text{st}}$  adiabatic invariant contours that is not visible in  
420 the overall mission set and in the GIRE3 predictions. As discussed, the proton fluxes and PSDs  
421 show little evidence of the initial impulse and, as the planet is approached, appear to be  
422 depressed although there is a peak at about  $L=12$ . The electrons, on the other hand, clearly show  
423 the impulsive event at  $L=15$  which drops off rapidly as the planet is approached followed by  
424 another impulse at the orbit of Europa.

425

426 To conclude, the Galileo EPD high energy electron and proton data and the GIRE3  
427 Jupiter environmental model both provide useful and consistent information on the variations of  
428 the jovian fluxes and PSDs for constant  $1^{\text{st}}$  adiabatic invariants. While both electrons and  
429 protons show a clear downward trend in flux and PSD at constant  $1^{\text{st}}$  adiabatic invariant as the  
430 planet is approached, the protons appear to fall off much more rapidly. This may indicate that  
431 the high energy protons are not diffusing inwards as fast as the electrons. While the GIRE3  
432 model predictions provide “mean” predictions of the electrons and protons from  $L=25$  well into  
433  $L=3$ , the Galileo data permit the study of orbit by orbit variations as exemplified by orbit C22.  
434 Finally, the Galileo data and the GIRE3 model potentially provide valuable inputs for studies of  
435 inward particle diffusion and energization at Jupiter.

436

#### 437 **Acknowledgements**

438

439 The research described in this paper was carried out at the Jet Propulsion Laboratory, California  
440 Institute of Technology, under a contract with the NASA (80NM0018D0004). The primary  
441 source and inspiration for this work was the authors’ friend and mentor, T. Neil Divine, who  
442 developed the initial programs and processes on which the GIRE model is based. The updates

443 would not have been possible without the significant contributions by personnel at JPL (R. W.  
444 Evans and J. M. Ratliff) and at the Johns Hopkins University Applied Physics Laboratory (e.g.,  
445 R. McEntire, D. Williams, C. Paranicas, and B. Mauk) who provided the energetic-particle-  
446 detector data from Galileo. The authors also thank J. E. P. Connerney and K. K. Khurana for  
447 allowing the use of their magnetic-field models. Finally, the authors owe special thanks to the  
448 Planetary Data System (S. Joy and others) who assisted in securing much of the data used here.  
449 Data used in this paper to create the figures will be uploaded to <https://data.nasa.gov> when the  
450 paper is accepted for publication.

451

452 © 2020 California Institute of Technology. Government sponsorship acknowledged.

453

## 454 **References**

455

456 Baker, D. N., and C. K. Goertz (1976), Radial diffusion in Jupiter's magnetosphere, *J. Geophys. Res.*, 81 (28), pp.  
457 5215-5219.

458

459 Cheng, A. F., C. G. MacLennan, L. J. Lanzerotti, M. T. Paonessa, and T. P. Armstrong (1983), Energetic ion losses  
460 near Io's orbit, *J. Geophys. Res.*, 88 (A5), pp. 3936-3944.

461

462 Cheng, A. F., S. M. Krimigis, and T. P. Armstrong (1985), Near equality of ion phase space densities at Earth,  
463 Jupiter, and Saturn, *J. Geophys. Res.*, 90 (A1), pp. 526-530

464

465 Connerney, J.E., M.H. Acuna, N.F. Ness, and T. Satoh (1998), New models of Jupiter's magnetic field constrained  
466 by the Io flux tube footprint, *J. Geophys. Res.*, 103 (A6), 11929–11940, 1998.

467

468 de Soria-Santacruz, M., Garrett, H. B., Evans, R. W., Jun, I., Kim, W., Paranicas, C., and Drozdov, A. (2016), An  
469 empirical model of the high-energy electron environment at Jupiter, *J. Geophys. Res.*, pp. 1-12, 2016. doi:  
470 10.1002/2016JA023059.

471

472 de Soria-Santacruz, M., Y. Y. Shprits, A. Drozdov, J. D. Menietti, H. B. Garrett, H. Zhu, A. C. Kellerman, and R. B.  
473 Horne (2017), Interactions between energetic electrons and realistic whistler mode waves in the Jovian  
474 magnetosphere, *J. Geophys. Res.*, 122, doi:[10.1002/2017JA023975](https://doi.org/10.1002/2017JA023975).

475

476 Divine, N. T., and H. B. Garrett (1983), Charged Particle Distributions in Jupiter's Magnetosphere, *J. Geophys. Res.*,  
477 88, 6889-6903.

478

479 Fieseler, P. D., S. M. Ardanian, and A. R. Frederickson (2002), The Radiation Effects on Galileo Spacecraft Systems  
480 at Jupiter, *IEEE Trans. Nuc. Sci.*, Vol. 49, No. 6.

481

482 Garrett, H. B., I. Jun, J. M. Ratliff, R. W. Evans, G. A. Clough, and R.W. McEntire (2003), Galileo Interim  
483 Radiation Electron Model, *JPL Publication 03-006*, 72 pages, The Jet Propulsion Laboratory, California  
484 Institute of Technology, Pasadena, CA.

485

486 Garrett, H. B., S. M. Levin, S. J. Bolton, R. W. Evans, B. Bhattacharya (2005), A revised model of Jupiter's inner  
487 electron belts: Updating the Divine radiation model, *Geophys. Res. Lett.*, Vol. 32, No. 4, L04104  
488 <http://dx.doi.org/10.1029/2004GL021986>.

489

490 Garrett, H. B., M. Kokorowski, I. Jun, and R. W. Evans (2012), Galileo Interim Radiation Electron Model Update—  
491 2012, *JPL Publication 12-9*. <https://trs.jpl.nasa.gov/handle/2014/42026>.

492

493 Garrett, H. B., Martinez-Sierra, Luz Maria, and Evans, R. W. (2015), Updating the Jovian Proton Radiation  
494 Environment—2015, *JPL Publication 15-9*, pp. 36, <http://hdl.handle.net/2014/45463>.

495

496 Garrett, H. B., W. Kim, and R. W. Evans, (2016), Updating the Jovian Plasma and Radiation Environments: The  
497 Latest Results for 2015, *Journal of Spacecraft and Rockets*, pp. 1-15. doi: 10.2514/1.A33510  
498

499 Garrett, H. B., I. Jun, R. W. Evans, W. Kim, and D. Brinza, (2017), The Latest Jovian-Trapped Proton and Heavy  
500 Ion Models”, *IEEE Trans. Nuc. Sci.*, Vol. 64, Issue 11, pp. 2802–2813, doi 10.1109/TNS.2017.2755618.  
501

502 Jun, I., J. M. Ratliff, H. B. Garrett, and R. W. McEntire (2002), Monte Carlo simulations of the Galileo Energetic  
503 Particle Detector, *Nuc. Instr. and Methods in Phys. Res., A*, Vol. 490, 465-475.  
504

505 Jun, I., H. B. Garrett, R. Swimm, R. W. Evans, and G. Clough (2005), Statistics of the variations of the high-energy  
506 electron population between 7 and 28 jovian radii as measured by the Galileo spacecraft, *Icarus*, Vol. 178,  
507 pp. 386-394, doi:10.1016/j.icarus.2005.01.022.  
508

509 Jun, I., H. B. Garrett, and R. W. Evans (2019), Trapped Electron Environments of the Outer Planets, *IEEE Trans.*  
510 *Plasma Sci.*, Vol. 47, No. 8, pp, 3923-3930, doi: 10.1109/TPS.2019.2907069 .  
511

512 Khurana, K. K., and H. K. Schwarzl (2005), Global structure of Jupiter’s magnetospheric current sheet, *J. Geophys.*  
513 *Res.*, 110 (A07227). doi:10.1029/2004JA010757.  
514

515 Mauk, B. H., D. G. Mitchell, R. W. McEntire, C. P. Paranicas, E. C. Roelof, D. J. Williams, S. M. Krimigis, and A.  
516 Lagg (2004), Energetic ion characteristics and neutral gas interactions in Jupiter’s magnetosphere, *J.*  
517 *Geophys. Res.*, 109, A09S12, doi:10.1029/2003JA010270.  
518

519 McIlwain, C. E., and R. W. Fillius (1975), Differential Spectra and Phase Space Densities of Trapped Electrons at  
520 Jupiter, *J. Geophys. Res.*, Vol. 80, No. 10, pp. 1341-1345.  
521

522 Mogro-Campero, A., and W. Fillius (1976), The absorption of trapped particles by the inner satellite of Jupiter and  
523 the radial diffusion coefficient of particle transport, *J. Geophys. Res.*, 81 (7), pp. 1289-1295.  
524

525 Nenon, Q., A. Sicard, P. Kollman, H. B. Garrett, S. P. A. Sauer, and C. Paranicas (2018), A Physical Model of the  
526 Proton Radiation Belts of Jupiter Inside Europa’s Orbit, *J. Geophys. Res.: Space Physics*, 123, 3512–3532,  
527 <https://doi.org/10.1029/2018JA025216>.  
528

529 Roederer, J. G. (1970), Dynamics of geomagnetically trapped radiation”, *Springer-Verlag*, New York, New York,  
530 166 p.  
531

532 Thomsen, M. F., C. K. Goertz, and J. A. Van Allen (1977), On determining magnetospheric diffusion coefficients  
533 from the observed effects of Jupiter’s Satellite Io, *J. Geophys. Res.*, 82 (35), pp. 5541-5550.  
534

535 Williams, D. J., R. W. McEntire, S. Jaskulek, and B. Wilken (1992), The Galileo Energetic Particle Detector, in *The*  
536 *Galileo Mission*, edited by C.T. Russell, pp. 385–412, Kluwer Academic Publishers, Dordrecht, The  
537 Netherlands.  
538

539 Woodfield, E. E., R. B. Horne, S. A. Glauert, J. D. Menietti, and Y. Y. Shprits (2014), The origin of Jupiter’s outer  
540 radiation belt, *J. Geophys. Res. Space Physics*, 119, pp. 3490–3502, 2014, doi:10.1002/2014JA019891.